ACCOUNTS
of chemical research

Discrete Cyclic Porphyrin Arrays as Artificial Light-Harvesting Antenna

NAOKI ARATANI,[†] DONGHO KIM,[*,‡] AND ATSUHIRO OSUKA[*,†]

[†]*Department of Chemistry, Graduate School of Science, Kyoto University, Sakyo-ku, Kyoto 606-8502, Japan, and* [‡]*Spectroscopy Laboratory for Functional π-Electronic Systems, and Department of Chemistry, Yonsei University, Seoul 120-749, Korea*

RECEIVED ON JUNE 8, 2009

CONSPECTUS

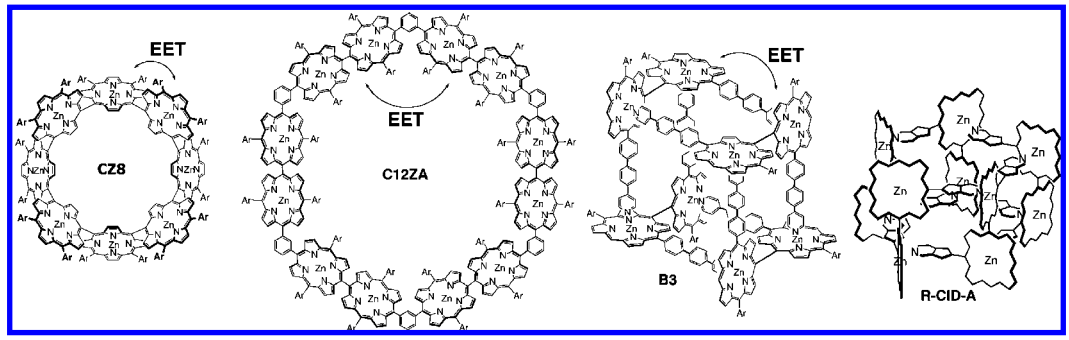

The importance of photosynthesis has driven researchers to seek ways to mimic its fundamental features in simplified systems. The absorption of a photon by light-harvesting (antenna) complexes made up of a large number of protein-embedded pigments initiates photosynthesis. Subsequently the many pigments within the antenna system shuttle that photon via an efficient excitation energy transfer (EET) until it encounters a reaction center. Since the 1995 discovery of the circularly arranged chromophoric assemblies in the crystal structure of light-harvesting antenna complex LH2 of purple bacteria *Rps. Acidophila*, many designs of light-harvesting antenna systems have focused on cyclic porphyrin wheels that allow for efficient EET.

In this Account, we review recent research in our laboratories in the synthesis of covalently and noncovalently linked discrete cyclic porphyrin arrays as models of the photosynthetic light-harvesting antenna complexes. On the basis of the silver(I)-promoted oxidative coupling strategy, we have prepared a series of extremely long yet discrete *meso*−*meso*-linked porphyrin arrays and covalently linked large porphyrin rings. We examined the photophysical properties of these molecules using steady-state absorption, fluorescence, fluorescence lifetime, fluorescence anisotropy decay, and transient absorption measurements. Both the pump-power dependence on the femtosecond transient absorption and the transient absorption anisotropy decay profiles are directly related to the EET processes within the porphyrin rings. Within these structures, the exciton−exciton annihilation time and the polarization anisotropy rise time are well-described in terms of the Förster-type incoherent energy hopping model.

In noncoordinating solvents such as $CHCl_3$, *meso*-pyridine-appended zinc(II) porphyrins and their *meso*−*meso*-linked dimers spontaneously assemble to form tetrameric porphyrin squares and porphyrin boxes, respectively. In the latter case, we have demonstrated the rigorous homochiral self-sorting process and efficient EET along these cyclic porphyrin arrays. The *meso*-cinchomeronimide appended zinc(II) porphyrin forms a cyclic trimer. We have also shown that the corresponding *meso*−*meso*-linked diporphyrins undergo high-fidelity self-sorting assembling to form discrete cyclic trimer, tetramer, and pentamer with large association constants through perfect discrimination of enantiomeric and conformational differences of the *meso*-cinchomeronimide substituents. Collectively, these studies of covalently and noncovalently linked discrete cyclic porphyrin arrays aid in the understanding of the structural requirements for such very fast EET in natural light-harvesting complexes.

Published on the Web 10/20/2009 www.pubs.acs.org/acr
10.1021/ar9001697 CCC: $71.50

Introduction

The importance of photosynthesis has driven many researchers to look for ways to duplicate the fundamental features of photosynthesis in simplified systems. Photosynthesis is initiated by the absorption of a photon by light-harvesting (antenna) complexes that usually comprise a large number of pigments embedded in protein matrixes. This process is followed by an efficient excitation energy transfer (EET) over many pigments within the antenna system until a reaction center is encountered.

In 1995, the crystal structure of light-harvesting antenna complex LH2 of purple bacteria *Rps. acidophila* was elucidated to be circularly arranged chromophoric assemblies.[1] LH2 consists of two wheel-like pigment arrays; B800 with 9 bacteriochlorophyll *a* (Bchl *a*) and B850 with 9 dimeric subunits (totally 18 pigments) of Bchl *a*. Since the advent of this wheel-like structure, the designs of light-harvesting antenna systems have been revolutionized to focus on cyclic porphyrin wheels that allow the efficient EET in a cyclic manner. The large and shape-persistent structures of such porphyrin wheels have also evoked different interests in fields of host−guest chemistry, single molecular photochemistry, and so on. In this account, we focus on our own recent developments of cyclic porphyrin arrays with a particular attention on *meso*−*meso* directly linked arrays. The electronic coupling between the constituent porphyrin chromophores is a key parameter that controls various important photophysical functions of porphyrin arrays. In most cases, porphyrin arrays are not π-conjugated and only weakly electronically coupled via through-space and through-bond interactions, while some of these arrays exhibit excitonic interactions depending on their orientation and distance between the porphyrin units. For example, rigid aromatics-bridged porphyrin dimers have been shown to be useful for the tuning of the exciton coupling and the rates of intramolecular energy-/electron-transfer reactions, since the geometry of two porphyrin rings can be precisely controlled.[2]

We have explored a variety of covalently and noncovalently assembled cyclic porphyrin arrays mainly as biomimetic models of light-harvesting antenna in photosynthetic systems. The key reaction is the Ag(I)-promoted coupling reaction of 5,15-diaryl zinc(II) porphyrin that provides a *meso*−*meso*-linked diporphyrin regioselectively (Scheme 1).[3] Synthesis of *meso*−*meso*-linked diporphyrins opened a new synthetic porphyrin chemistry, in which metalloporphyrins with free *meso* positions are converted under appropriate oxidation conditions into a variety of directly linked porphyrin arrays with varying electronic interactions. An advantage of this coupling reaction is its extremely easy extension to higher porphyrin arrays, since longer porphyrin arrays have practically the same reactivity as that of the monomer. On the basis of this strategy, we have prepared a wide range of covalently linked diporphyrins and porphyrin arrays, including *meso*−*meso*-linked linear porphyrin arrays,[4] two-dimensional windmill arrays,[5] three-dimensional gridlike arrays,[6] and cyclic arrays,[7−9] which are interesting as artificial antenna models in terms of the well-defined arrangement of many porphyrins (Scheme 1). Efficient EET along these porphyrin arrays has been revealed by the time-resolved transient absorption and fluorescence measurements.

SCHEME 1. A List of *meso*−*meso*-Linked Porphyrin Arrays

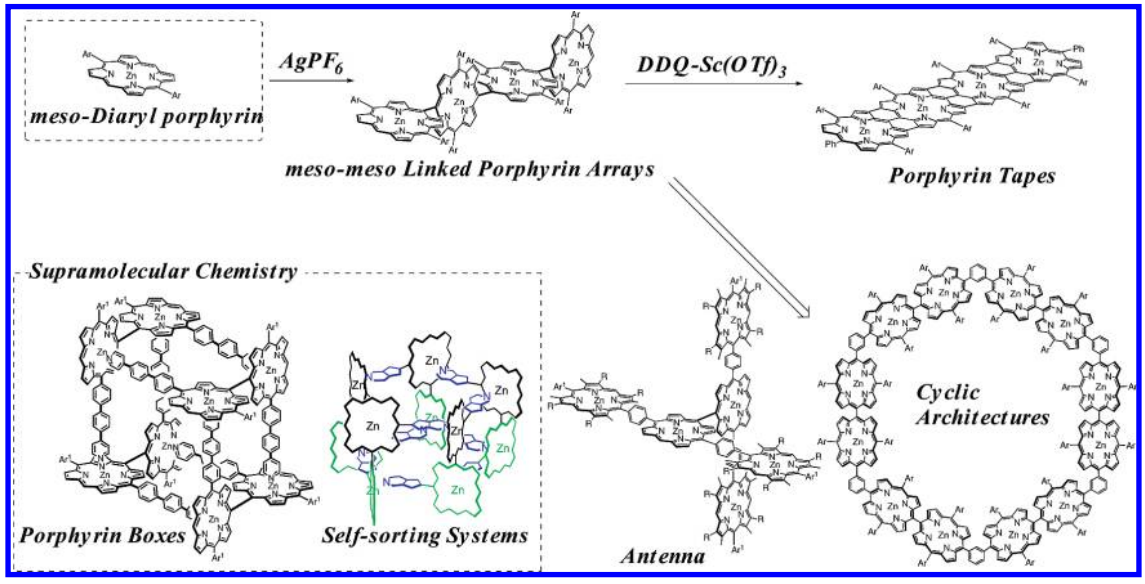

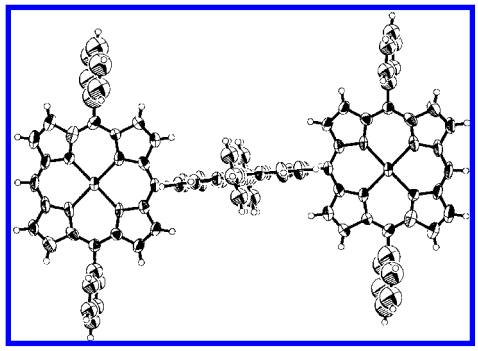

FIGURE 1. X-ray crystal structure of *meso*−*meso*-linked porphyrin trimer.

Discussion and Results

Oxidative Coupling Reaction and Transition-Metal Catalyzed Cross-Coupling Reaction. After the pioneering work of Sanders and Anderson in 1989,[10] several cyclic porphyrin arrays have been reported, in which each porphyrin is connected by covalent bonds.[9] However, the linkages have been limited to aryl- or alkynyl-based *meso*-substituents, rendering the intramolecular excitonic interaction between the neighboring chromophores to remain small. In contrast, *meso*−*meso* directly linked porphyrin arrays possess a distinct advantage that they are directly linked and are favorable for achieving rapid energy- and electron-transfer reactions owing to a short center-to-center distance (ca. 8.4 Å) and large excitonic interaction (Figure 1).[11] A nearly orthogonal conformation minimizes the π-conjugation of neighboring porphyrins, making a state-to-state dynamic energy- and/or electron-transfer process feasible without causing serious electronic delocalization.

The silver(I)-prompted oxidative coupling reaction is highly regioselective, occurring only at the *meso* position. A zincated porphyrin monomer substrate is favorable for the coupling reaction owing to its low oxidation potential. In each coupling step, dimerized, trimerized, and tetramerized compounds were obtained constantly in 20−30%, ∼13%, and ∼6% yields, respectively, along with the recovery of starting materials (50−55%). Highly regioselective coupling is ascribed to the large electron density at *meso*-positions in the highest occupied molecular orbital (HOMO) of a zinc porphyrin radical cation. To obtain oligomers with a desired number of porphyrins, reaction conditions should be carefully controlled for concentration, equivalent of Ag(I) salt, temperature, and reaction time. The remarkable advantages of this coupling reaction are (1) its easy repeatability owing to practically the same coupling reactivities of longer *meso*−*meso*-linked porphyrin arrays and (2) high solubilities of long porphyrin arrays. Coupling products were separated through preparative GPC−HPLC by taking advantage of a large difference in the retention time. The longest *meso*−*meso*-linked porphyrin arrays thus synthesized is 1024-mer, which is an extremely long monodisperse molecule with a molecular length of ca. 0.84 μm.[11]

SCHEME 2. Synthetic Routes for the Construction of Various Shaped Porphyrin Arrays

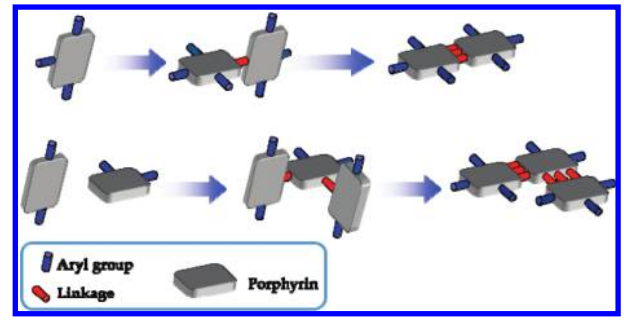

The silver(I)-promoted oxidative coupling reaction is particularly effective in the homocoupling of zinc(II) porphyrins but is not applicable to heterocoupling of different porphyrins. To complement this, we developed a *meso*−*meso* hetero(cross)-coupling of different porphyrins by means of transition metal-catalyzed reactions (typically 60−80% yield in each C−C bond formation) (Scheme 2).[12] Porphyrins have been merely recognized as a reaction substrate in transition metal-catalyzed transformations. Recently, application of such methodologies to porphyrin synthesis has proven to be very powerful in creating new types of porphyrin arrays, which have their own intriguing structures and properties.[13] New transformations of porphyrins via transition metal catalysis offer us prospects of new designs of architectures, thus facilitating further development of this important class of functional molecules.[14,15]

We have also reported that further oxidation of singly *meso*−*meso*-linked porphyrin arrays under stronger oxidative conditions (DDQ and $Sc(OTf)_3$) provided *meso*−*meso*, β−β, β−β, triply linked porphyrin arrays (porphyrin tapes), whose Q-like bands, the lowest electronic absorption bands, exhibit continuous red-shifts, reaching deeply into the infrared region because of the extensive π-conjugation over the molecules (Figure 2).[15,16]

Excitonic Interaction in *meso*−*meso* Directly Linked Porphyrin Arrays. EET processes are the most important function of antenna complexes. Thus, many artificial model compounds have been explored, which absorb visible light in a wide range and funnel the resulting excited-state energy rapidly and efficiently to a designed site. The electronic interactions of neighboring porphyrin chromophores in the arrays are the key parameters for EET. Such interactions can be evaluated from their absorption spectra. The simple point-dipole

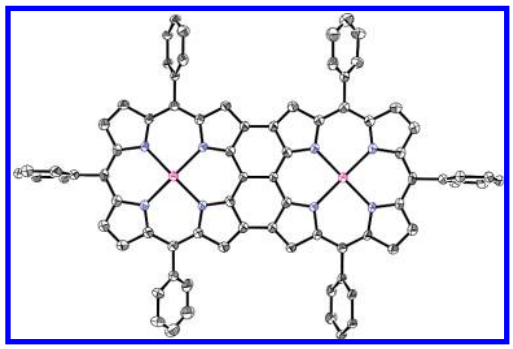

FIGURE 2. X-ray crystal structure of a porphyrin tape.

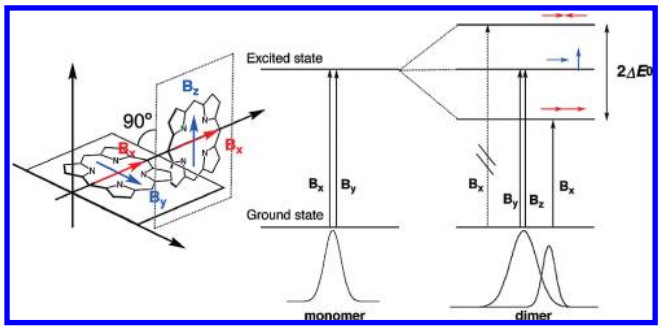

FIGURE 3. Schematic diagram of the excitonic interaction in *meso*−*meso*-linked diporphyrin.

exciton coupling theory developed by Kasha is useful to interpret the spectral changes caused by the interchromophore interactions, where the strength of dipole interaction is represented by Coulombic interactions that depend on the oscillator strength, orientation, and distance.[17] Interaction of transition dipole moments in a head-to-tail arrangement results in an optically allowed lower energy transition (J-type coupling), while that in a parallel arrangement results in an optically allowed higher energy transition (H-type coupling). Characteristically, *meso*−*meso*-linked porphyrin arrays exhibit split Soret bands due to J-type exciton coupling (Figure 3). The components of Soret band, B_x and B_y, which are degenerate in a porphyrin monomer, independently interact with the transition dipole moments of neighboring porphyrins. B_x transition dipole moments along the *meso*−*meso* bond are excitonically coupled to generate an allowed lower energy transition ($B_x + B_x$), while the mutual Coulombic interactions between B_x and B_y (or B_z) transition dipole moments are noninteracting owing to their orthogonal orientation. Consequently, the Soret band of *meso*−*meso*-linked linear porphyrin arrays is split into a red-shifted band and an unperturbed one.

***meso*−*meso* Directly Linked Cyclic Porphyrin Arrays.**[18] It is expected that the regular cyclic arrangement and the large electronic coupling between neighboring pigments are required for efficient EET. Cyclic porphyrin architectures, in which the constituent porphyrins are all directly linked at *meso*−*meso* positions, were an attractive target in view of synthetic challenge, higher molecular symmetry, and large and regular electronic interactions between neighboring porphyrins that lead to efficient EET. Such molecules can be regarded as genuine porphyrin rings whose π-electronic network consists of only porphyrins.

We have synthesized the directly linked cyclic porphyrin arrays starting from 5,10-diaryl zinc porphyrin monomer **1** (Scheme 3). By Ag(I)-salt oxidation, dimer **2** (24% yield) and trimers **3a** and **3b** (totally 7% yield) were obtained from **1**, and tetramers **4a** and **4b** (totally 40% yield) were obtained from **2**. In these oligomers, free rotation around *meso*−*meso* linkage is strictly prohibited because of steric hindrance. Among them, **3a** and **4a** that have unsubstituted *meso*-positions in the same side are suitable precursors for cyclic arrays. Cyclic tetramer **CZ4** was synthesized in 74% yield by the intramolecular coupling reaction of **4a** at [**4a**] = 2×10^{-5} M, whereas the major product was changed to be cyclic octamer **CZ8** (29%) at [**4a**] = 3.3×10^{-3} M. Cyclic hexamer **CZ6** was synthesized in 22% yield from the coupling reaction of **3a** at [**3a**] = 1.0×10^{-4} M. These cyclic arrays were separated by silica-gel column chromatography, and their structures were fully consistent with their ^{1}H NMR spectra, which are characteristically simple without *meso*-proton signals, reflecting the symmetric cyclic structures.

In contrast to the linear *meso*−*meso* linked porphyrin arrays, directly *meso*−*meso* linked cyclic porphyrin arrays exhibit a broad Soret band at red-shifted Soret band position. In the cyclic arrays, both the transition dipole moments B_x and B_y are excitonically coupled with those of the neighboring porphyrins to cause an excitonically allowed state of the same energy. As described above, the linear *meso*−*meso*-linked porphyrin arrays exhibit J-type exciton coupling along the long molecular axis, but H-type coupling is also possible when the array is bent as seen for **CZ4** and **CZ8**, in which the dihedral angles of neighboring porphyrin rings are deviated from 90°.

The EET rates in **CZ4**, **CZ6**, and **CZ8** were determined by the transient absorption (TA) and transient absorption anisotropy (TAA) measurements. In TA measurements, pump-power dependent decay causes the singlet−singlet excitation annihilation process due to Förster-type incoherent EET within the array. EET processes in the directly linked cyclic arrays are quite efficient with the rate constants of $(119\ \text{fs})^{-1}$ for **CZ4**, $(342\ \text{fs})^{-1}$ for **CZ6**, and $(236\ \text{fs})^{-1}$ for **CZ8**, which rival those in B850 of a natural cyclic antenna system. These efficient EET processes are arising from extremely strong excitonic coupling between porphyrin components. The observed order of EET rates of **CZ6** < **CZ8**

SCHEME 3. Synthesis of *meso*−*meso* Directly Linked Porphyrin Rings. Ar = 3,5-Di-*tert*-butylphenyl

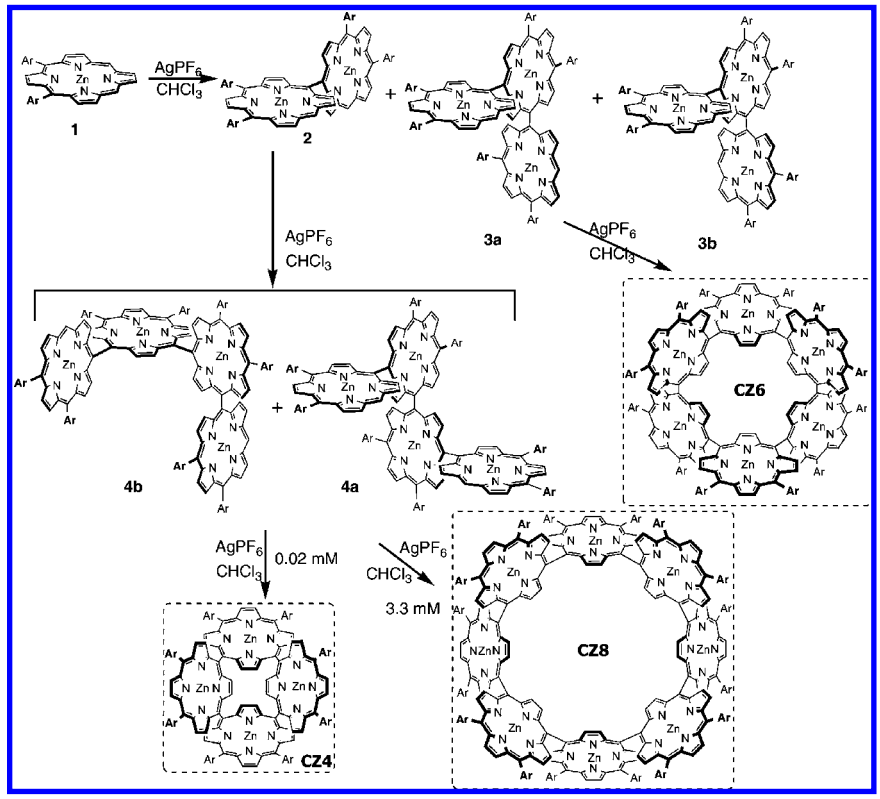

< **CZ4** is the same as the order of the electronic communication between neighboring porphyrin units, as estimated from their absorption spectra and calculated dihedral angles between neighboring porphyrins.

Another type of a *meso*−*meso* directly linked porphyrin octamer has been prepared by a Pd-catalyzed coupling reaction in a stepwise designed manner.[14] This strategy is useful for the preparations of hybrid porphyrin arrays with definite compositions and unique molecular shapes.

***m*-Phenylene-Linked Porphyrin Wheels.**[19−21] Wheel-like porphyrin oligomers were also synthesized from 1,3-phenylene-bridged *meso*−*meso*-linked porphyrin oligomers. Dimer **2ZA** and tetramer **4ZB** were prepared by the Suzuki coupling reaction of a *meso*-boronated zinc porphyrin and a *meso*-boronated zinc diporphyrin with 1,3-diiodobenzene, respectively. Repetitive oxidation reactions starting from bridged porphyrin dimer **2ZA** gave linear 12-mer **12ZA**. Using the same reaction procedure, linear precursor 24-mer **24ZB** was obtained from bridged porphyrin tetramer **4ZB**. These acyclic porphyrin arrays were then cyclized by intramolecular coupling under highly diluted conditions (1×10^{-6} M) (Schemes 4 and 5). Cyclic compounds were isolated by preparative recycling GPC−HPLC in 60% yield for **C12ZA** and in 34% yield for **C24ZB**. The cyclic structure of **C12ZA** was confirmed by its ^{1}H NMR spectrum that lacked the *meso* proton signals, but the ^{1}H NMR spectrum of **C24ZB** was rather broad, probably due to structural heterogeneity of such a large molecule.

UV−vis absorption spectra of **C12ZA** and **C24ZB** are similar to those of dimer **Z2** and tetramer **Z4** components, respectively, while the further split Soret bands of **C12ZA** indicate additional dipole−dipole interaction between **Z2** subunits via the 1,3-phenylene spacer (Figure 4). These data indicate that the electronic interactions are predominated by the exciton coupling within *meso*−*meso* linked porphyrin subunits. Significant differences in the absorption spectra between acyclic arrays and cyclic arrays are shoulder peaks in the spectra of **12ZA** and **24ZB**, which correspond to terminal monomer or dimer moiety, respectively, and are not observed in the spectra of the cyclic arrays **C12ZA** and **C24ZB**.

The EET rates in **C12ZA** and **C24ZB** have been determined similarly by TA and TAA to be $(3.6\ \text{ps})^{-1}$ and $(35\ \text{ps})^{-1}$, respectively.[19−21] These rates are almost the same as those of the respective references, **4ZB** and **8ZC** (Scheme 5). In these arrays, the excited state is considered to be delocalized over the dimeric or tetrameric porphyrin subunit. On the basis of these data, a Förster-type EET model was used to interpret the EET processes in **C12ZA** and **C24ZB**. A large difference between EET rates of **C12ZA** and

SCHEME 4. Synthesis of *m*-phenylene Linked Cyclic Porphyrin Dodecamer. Ar = 4-Dodecyloxyphenyl

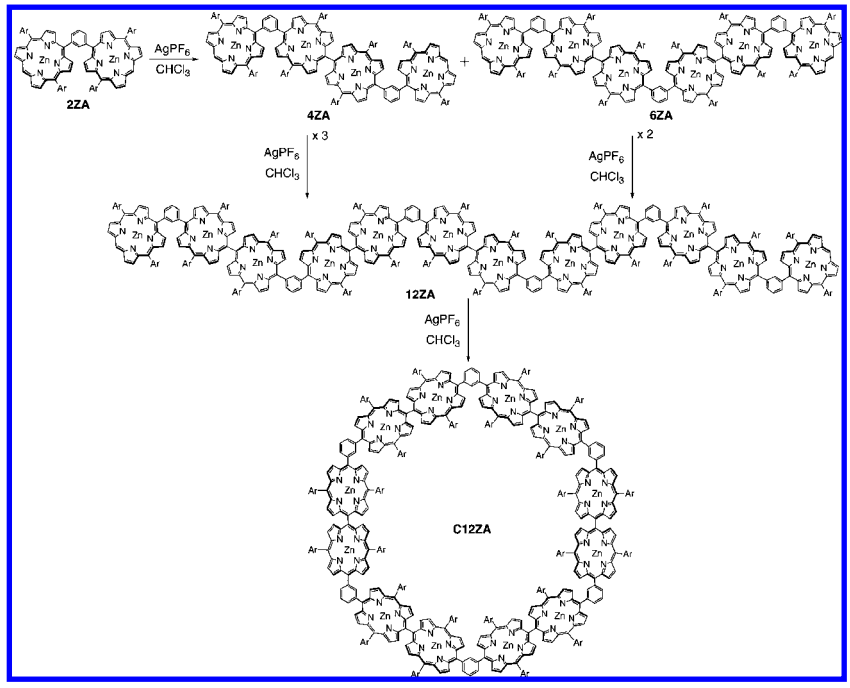

SCHEME 5. Synthesis of *m*-Phenylene Linked Cyclic Porphyrin 24-mer. Ar = 4-Dodecyloxyphenyl

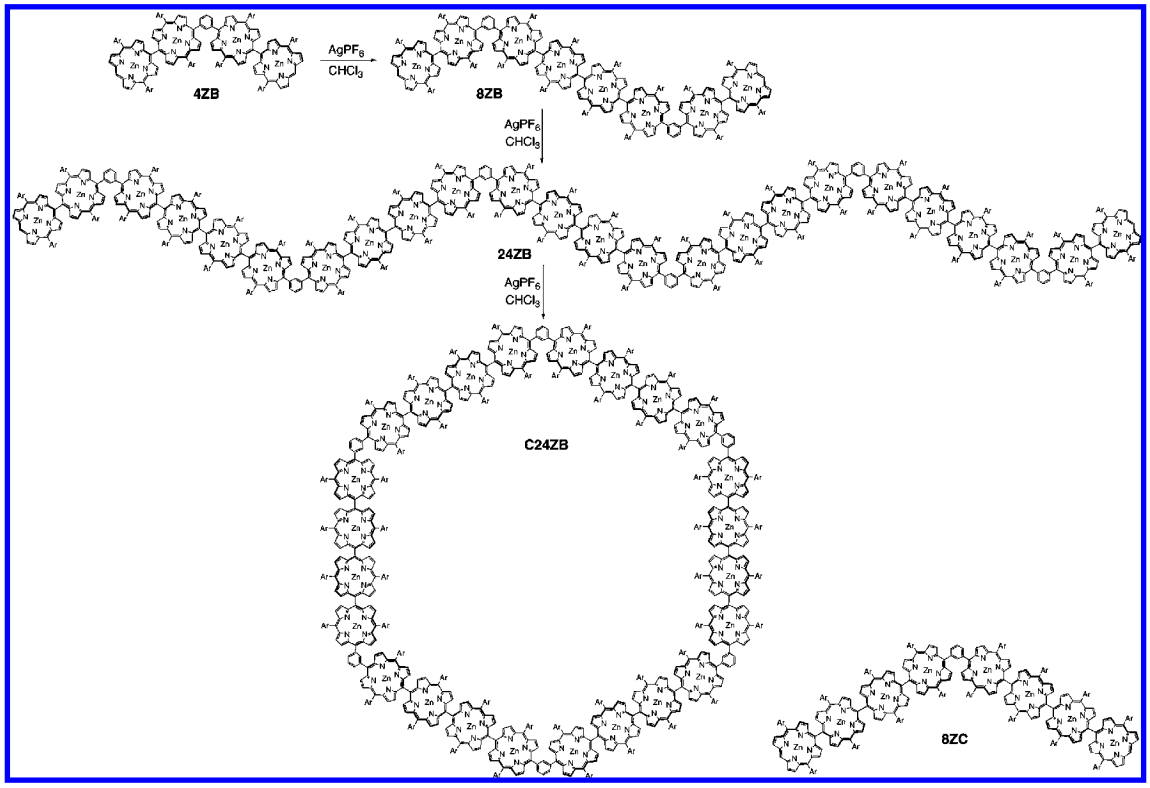

C24ZB is explained in terms of a large difference in the center-to-center distance of *meso*−*meso*-linked porphyrin subunits. The distance of **C24ZB** is ca. 1.5-fold longer than that of **C12ZA**, which, on the basis of the distance factor of R^{-6} in the Förster EET equation, explains well the approximately 10 times difference in the observed EET rate.

By the way, as the crystal structure of LH1 has been revealed to possess BChl *a* wheel composed of 15 pairs of

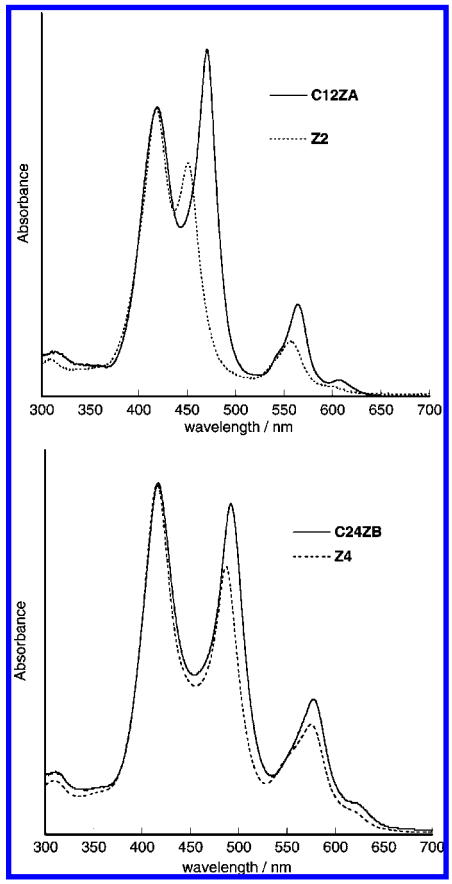

FIGURE 4. Steady-state absorption spectra of (a) **C12ZA** and (b) **C24ZB** in THF, to which the absorption spectrum of zinc(II) 5,15-bis(4-dodecyloxyphenyl)porphyrin dimer (**Z2**) and tetramer (**Z4**) was added for comparison.

dimeric subunits (total 30 BChl *a* molecules),[22] this gigantic structure has encouraged further synthetic efforts toward even larger cyclic porphyrin arrays. We have reported the synthesis of longer 1,3-phenylene-bridged porphyrin arrays and their intramolecular cyclization reactions to large porphyrin wheels. The porphyrin wheel **C32ZA** comprises 32 porphyrin subunits, which is, to the best of our knowledge, the largest porphyrin ring reported so far.[23]

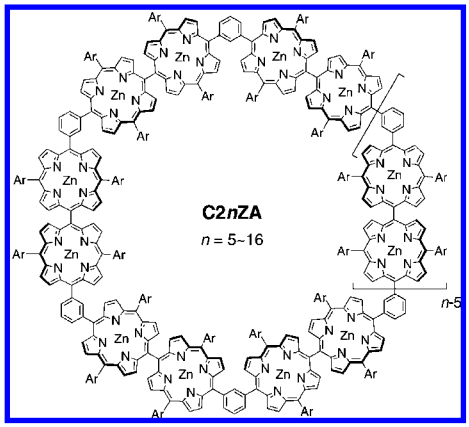

Assembling via Self Sorting—Key Features for Molecular Design of Self-Assembly. The use of noncovalent supramolucular interactions has been shown to be beneficial, particularly toward construction of cyclic porphyrin arrays owing to intrinsic dynamic nature and entropic gain associated with formation of distinct molecular assemblies rather than polymeric assemblies. Some pioneering works were reported by Hunter et al.,[24] and recently Kobuke reported the formation of cyclic porphyrin assemblies from 5-imidazoyl-substituted porphyrin dimers, which are bridged by a 1,3-phenylene spacer.[25]

An advantage of these coordinatively bonded arrays is their relatively easy synthetic accessibility, in that appropriately designed components are almost automatically self-assembled to form large arrays. This assembling process is especially effective for the construction of a discrete cyclic array owing to the associated entropic advantage. Spatial control of porphyrinic pigments is crucial in supramolecular design, since it directly leads to control of the electronic interactions between chromophores. In this respect, a precise spatial control of porphyrin pigments with ample electronic interactions still remains challenging. For use as light-harvesting antennae, careful avoidance of an energy sink that deactivates the excited state is another important requirement.

To construct the desired molecular assembly, an inclination between the porphyrin plane and the ligand plays a key role. Changing the geometry of the monomer unit can have dramatic effects on the structure and self-assembly properties.

Self-sorting recognition with high fidelity is a common and fundamental property in biological systems. A self-sorting assembling process with discrimination of subtle structural differences among similar isomers may lead to largely different tertiary architectures of variable functions. Structural diversity thus attained plays an important role in many biological processes. Protein and DNA build complicated systems to pass through a precise correct molecular recognition process and seek out a partner. Aggregates formed via self-sorting processes are mainly built thermodynamically through noncovalent bonds such as hydrogen bonds, metal coordination interactions, or hydrophobic interactions. In recent years, therefore, diverse efforts have been made toward synthetic supramolecular systems that achieve such high fidelity self-sorting assemblies.[26]

Metalloporphyrins bearing a coordinating side arm have been used as an effective platform to build various supramolecular structures with the aid of multiple coordination interactions of central metal ions. However, such metalloporphyrins have been scarcely tested for a self-sorting process. Comple-

SCHEME 6. Supramolecular Porphyrin Squares **S1**−**S3**. Ar = 3,5-Dioctyloxyphenyl

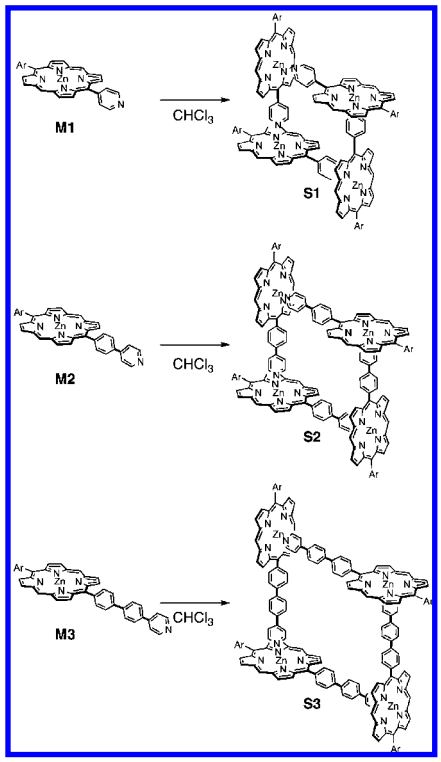

SCHEME 7. Supramolecular Porphyrin Boxes **B1**−**B3**. Ar = 3,5-Dioctyloxyphenyl

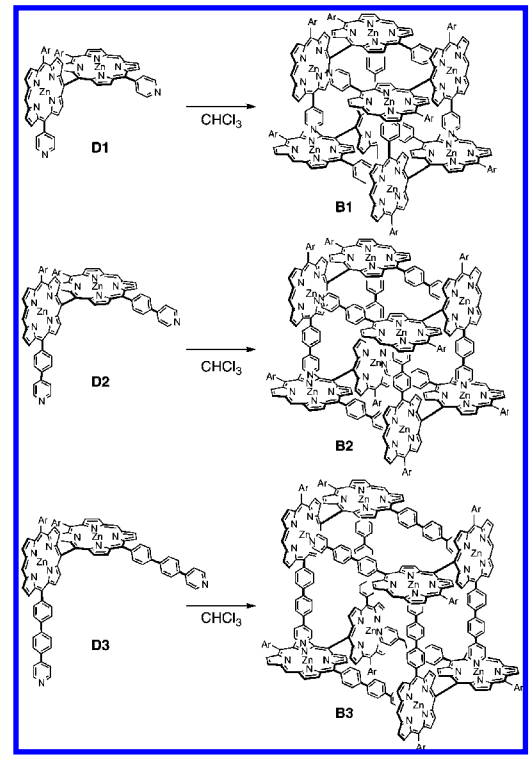

mentary multiple coordination interactions arising from a *meso*−*meso*-linked diporphyrin framework help increase the association constants, such that the aggregates can be manipulated like covalently linked molecules.

Porphyrin Boxes Constructed from *meso*−*meso* Linked Diporphyrins.[27,28] We have explored three-dimensional porphyrin boxes that are formed via rigorous enantiomeric self-sorting assembling of racemic 4-pyridine-appended *meso*−*meso*-linked Zn(II) diporphyrins, in which the structural matching of the 90° dihedral angle between the diporphyrin and the 4-pyridyl group plays a key role toward the formation of box-shaped assemblies.

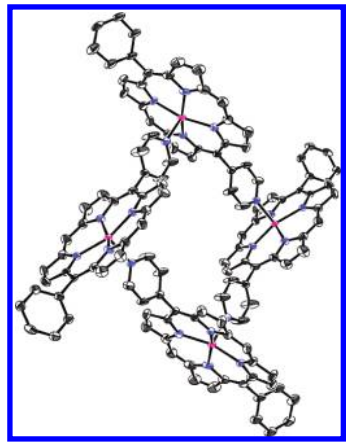

FIGURE 5. X-ray crystal structure of **S1**.

First, we showed that a series of 5-*p*-pyridyl-15-(3,5-dioctyloxyphenyl) zinc(II) porphyrin **M1**−**M3** form cyclic porphyrin tetramer **S1**−**S3** in noncoordinating solvents such as chloroform or benzene, which was confirmed by ^{1}H NMR spectra and UV−vis absorption spectra (Scheme 6). The related structure of 5-*p*-pyridyl-15-(3,5-di-*tert*-butylphenyl) zinc(II) porphyrin was also confirmed by X-ray crystal structure analysis (Figure 5).

The Ag(I)-promoted coupling reaction of **M1**−**M3** gave *meso*−*meso*-coupled diporphyrin **D1**−**D3** (36% yield for **D1**, 32% yield for **D2**, 20% yield for **D3**) along with higher oligomers. **D1** also aggregated to form a tetrameric conformation with a larger association constant and rigidity (Scheme 7). Quantitative self-assembly of **D1** as its tetramer **B1** was confirmed by ^{1}H NMR spectroscopy in $CDCl_3$ and cold spray ionization mass spectroscopy (CSI-MS). On the basis of the practical concentration independence of its fluorescence spectral shape (up to 1.0×10^{-8} M), the association constant of **B1** was estimated to be at least $>10^{25}$ M^{-3} in $CHCl_3$, indicating a rigid self-assembled structure. Formation of porphyrin boxes **B2** and **B3** from **D2** and **D3** was similarly confirmed by ^{1}H NMR spectra in $CDCl_3$.

Owing to the different *meso*-aryl substituents, **D1**−**D3** are all chiral, and hence, two enantiomers are present in equal abundance in solution. Accordingly, the chiral porphyrin boxes

SCHEME 8. Supramolecular Trimerization of **CIM** and its X-ray Crystal Structure. Ar = 3,5-Di-*tert*-butylphenyl

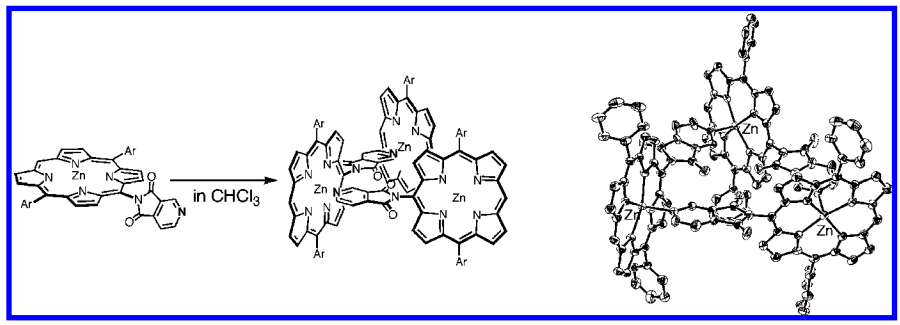

B1−**B3** are formed by homochiral self-sorting assembly of the respective (*R*) and (*S*) isomers of **D1**−**D3**. Actually the optical resolution of **B1** and **B2** has been accomplished with a chiral HPLC setup. The CD spectra of optically separated **B1** are similar to those of **B2**, but the intensity at 450 nm is doubled reflecting a shorter pyridyl arm, thus providing evidence for the exciton coupling between the noncovalent neighboring porphyrin rings.

EET processes within **B1**−**B3** have been investigated by the steady-state and time-resolved spectroscopic methods. Both the pump-power dependent TA and the TAA decay profiles have been directly associated with the EET processes within the **B1**−**B3** boxes. Consequently, the EET rates between the zinc(II) diporphyrin units have been estimated for **B1** (48 ps)$^{-1}$, **B2** (98 ± 3 ps)$^{-1}$, and **B3** (361 ± 6 ps)$^{-1}$.

***meso*-Cinchomeronimide Appended *meso*−*meso*-Linked Diporphyrin.**[29] As mentioned, one strategy to create assemblies of different shape is to displace the positions of coordinating nitrogen atoms from the porphyrin plane. This idea drove us to examine self-sorting assembling behaviors of 10,10′-cinchomeronimide-appended *meso*−*meso*-linked Zn(II) diporphyrin **CID**.

First, 10-cinchomeronimide-substituted 5,15-bis(3,5-di-*tert*-butylphenyl) Zn(II)- porphyrin **CIM** was prepared. ^{1}H NMR spectrum of **CIM** in $CDCl_3$ is very simple, featuring a simple set of peaks with large upfield shifts for the imide protons, which indicates the coordination of the pyridyl group to Zn(II) porphyrin (Scheme 8). The crystal structure of **CIM** revealed a triangular complex formed by complementary coordination of the cinchomeronimide group to the Zn(II) atom with a dihedral angle of 61° between the porphyrin mean planes (Scheme 8). The pyridyl group is coordinated to the zinc center with an angle of 88.8°, and the zinc center is displaced 0.272 Å out of the N4 plane that is slightly domed.

Next, *meso*−*meso*-linked diporphyrin **CID** bearing two cinchomeronimide groups at the 10,10′-position was prepared from 5,10-bis(3,5-di-*tert*-butylphenyl)porphyrin in 67% yield. Importantly, the free rotation of the cinchomeronimide group

SCHEME 9. Supramolecular Aggregation of **CID**. Ar = 3,5-Di-*tert*-butylphenyl

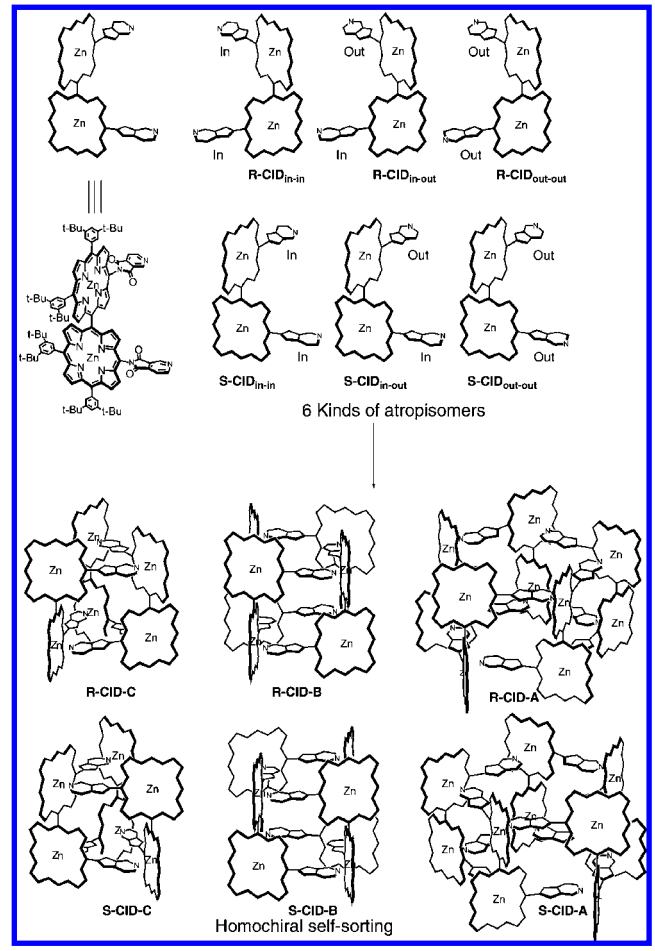

is considerably restricted because of the steric hindrance of the two imide-carbonyl groups, which gives rise to three different stable atropisomers (in−in, in−out, and out−out) with respect to the orientation of the nitrogen atom in the pyridine moiety. Prohibited rotation around the *meso*−*meso* linkage makes all the isomers to be chiral (*R* and *S*). Therefore, six isomers are present in a solution of **CID**; *R*-**CID$_{in-in}$**, *S*-**CID$_{in-in}$**, *R*-**CID$_{in-out}$**, *S*-**CID$_{in-out}$**, *R*-**CID$_{out-out}$**, and *S*-**CID$_{out-out}$** (Scheme 9).

The aggregates formed in $CHCl_3$ are stable enough to allow the separation by GPC. GPC analysis with polystyrene stan-

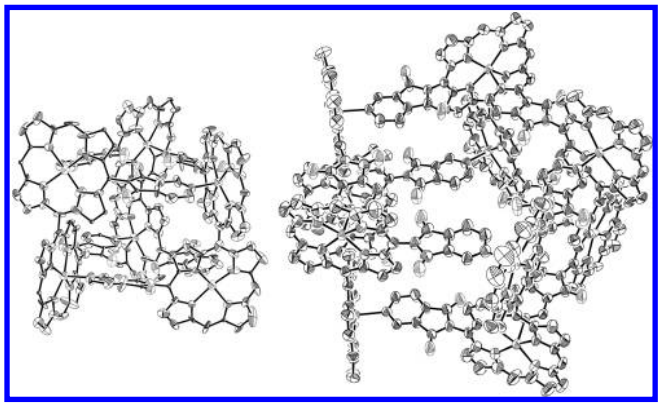

FIGURE 6. X-ray crystal structures of *R*-**CID-C** (left) and *R*-**CID-A** (right).

dards indicated the molecular weights, which roughly correspond to trimeric, tetrameric, and pentameric aggregates of three **CID**s.

X-ray diffraction analysis on *R*-$\mathbf{CID_{in\text{-}in}}$ shows that the trimer was constructed by complementary coordination of three molecules of an in−in conformer (*R*-**CID-C**) (Figure 6). The crystal structure on *R*-$\mathbf{CID_{out\text{-}out}}$ shows a symmetric pentameric aggregate consisting of five molecules of *R*-**CID-A** (Figure 6). The aggregate *R*-**CID-A** exhibits a C_5 symmetric pentagonal cylindrical structure with sides of ca. 11.5 Å and internal angles of ca. 108°. In the crystal, the aggregates *R*-**CID-A** are stacked in a tubular manner to form an infinite channel of ca. 10 Å diameter. Then, the aggregate form of $\mathbf{CID_{in-out}}$ was rationally assigned as a tetrameric aggregate **CID-B** composed of four molecules of an in−out conformer on the basis of its GPC retention time that indicated its molecular size to be larger than **CID-C** and smaller than **CID-A**.

Exclusive formation of the discrete cyclic aggregates without an appreciable amount of polymeric aggregate is also notable, which is probably driven by favorable entropic factors for formation of cyclic aggregates. Future studies will focus on incorporation of these functional units into more elaborate model systems and exploration of larger cyclic porphyrin arrays.

Single Molecular Spectroscopy of Cyclic Porphyrin Arrays. Single molecule fluorescence spectroscopy (SMFS) has emerged as a powerful tool to test the functionality of individual molecules over the past decade.[30] The substantial attention on SMFS is based not only on the single-molecule aspect of the technique, which gives unique information on distributions or time trajectories of the observables that are obscured in conventional techniques, but also on the optical probing feature that allows for the fewest perturbations of the object.

With these versatilities, many reports demonstrate how SMFS has contributed to the understanding of the excited-state dynamics of complex multichromophoric systems. However, the porphyrin-based molecular systems have scarcely been studied by SMFS due mainly to their low fluorescence quantum yields. Despite this, it is crucial to examine the photophysical properties of multiporphyrin systems at the single molecule level to directly observe salient behavior of individual molecules.

The fluorescence intensity trajectories (FITs), that is, the fluorescence intensity of a single molecule as a function of time, of **C12ZA** and **C24ZB** exhibit stepwise photobleaching behavior with fewer occurrences of off-times than those of linear dodecamer **12ZA**.[31] The frequent occurrence of long off-times in **12ZA** can be attributed to the existence of nonradiative decay channels, induced by the more flexible conformation of **12ZA**. On the other hand, the stepwise photobleaching observed in **C12ZA** and **C24ZB** is similar to the behavior observed in the FITs of other multichromophoric systems.

Coincidence measurements were carried out on single molecules of **12ZA**, **C12ZA**, and **C24ZB** to estimate the energy migration efficiency via S_1-S_1 annihilation processes. The S_1-S_1 annihilation can be understood in terms of simultaneous formation of two or more singlet excitons by the sequential absorption, within one intense laser pulse, of at least two photons in a cyclic porphyrin array (Figure 7a). The two or more singlet excitons quickly relax to the ground state to produce a more excited exciton through a collisional process that is mediated by consecutive energy migration along the cyclic array ($S_1 + S_1 \rightarrow S_n + S_0$), after which the higher excited exciton relaxes to the S_1 state via a fast internal conversion process. Consequently, the observed number of S_1 fluorescence photons is a direct indication of the efficiency of Förster-type resonance energy transfer (FRET). On the other hand, in solution, this collisional quenching of multiexcitons through EET processes results in additional fast decay components in the pump-power dependent TA decay profiles, which gives information on the EET time and efficiency (Figure 7b). In the interphoton arrival time distribution, the central peak (N_C) at 0 ns corresponds to two photons by the same laser pulse. In all other cases, interphoton arrival times are distributed in lateral peaks (N_L). As shown in Figure 7c, **C12ZA** exhibits a very small central peak compared to the lateral peaks, which is commonly observed for single-photon emitting systems, indicating that S_1-S_1 annihilation readily occurs by efficient FRET.

The N_C/N_L ratio (integrated values of central N_C peak divided by averaged ones of lateral N_L peaks in Figure 7c) in the interphoton arrival time distribution can be used to

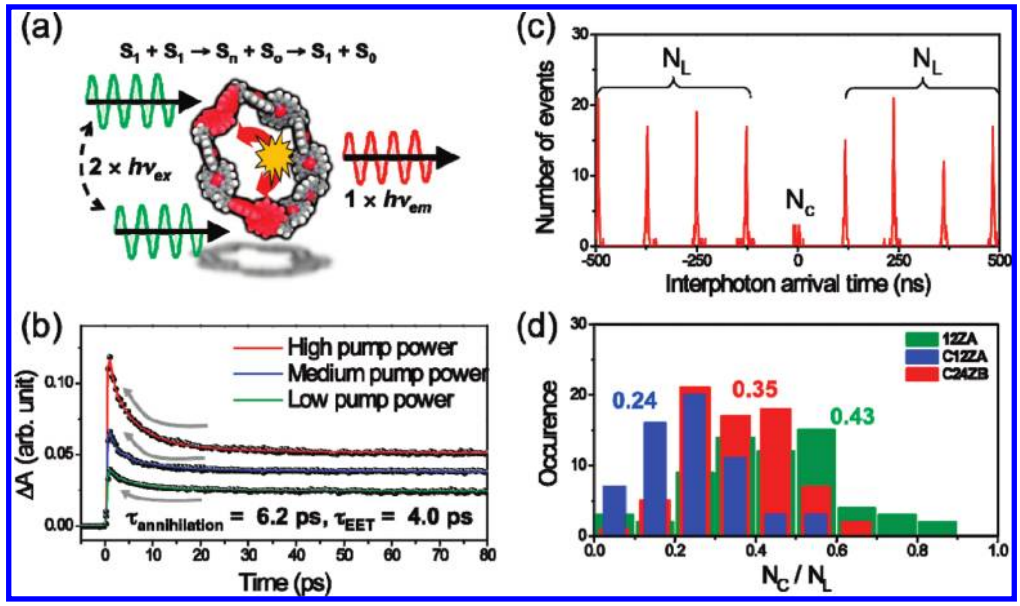

FIGURE 7. (a) Schematic diagram of S_1-S_1 annihilation processes observed in bulk solution and at single molecular level by using (b) pump-power dependent transient absorption decay and (c) coincidence measurement, respectively, for **C12ZA**; (d) histograms of N_C/N_L values for single molecules with their averaged values.

estimate the number of emitting porphyrin units in the multiporphyrin arrays, with a value of 0 corresponding to a single-photon emitter and 0.5 corresponding to a two-photon emitter. Larger values infer even less efficient S_1-S_1 annihilation processes. The mean N_C/N_L value of the linear array **12ZA** exhibits 0.43 with the large standard deviation. This feature suggests less efficient S_1-S_1 annihilation as well as larger conformational heterogeneity in **12ZA**. Indeed, **C12ZA** and **C24ZB** exhibit reduced mean N_C/N_L values of 0.24 and 0.35, respectively (Figure 7d). The smaller N_C/N_L value for **C12ZA** than that for **C24ZB** illustrates that **C12ZA** can be considered as a well-defined cyclic structure for efficient FRET processes. The structural distortion in **C24ZB** might reduce the energy migration efficiency by introducing competitive nonradiative decay channels. Since **C12ZA** is attested to exhibit more efficient energy migration processes than **C24ZB** due to the strong dipole−dipole interactions between diporphyrin subunits, we have extended our investigation on a series of cyclic porphyrin arrays **C10ZA**, **C12ZA**, **C16ZA**, **C18ZA**, **C24ZA**, and **C32ZA** composed of diporphyrin as a building block element.[32] In the histograms of the fluorescence lifetimes corresponding to all the detected photons at the initial emissive level in FITs, the distributions of the large cyclic porphyrin arrays **C18ZA**, **C24ZA**, and **C32ZA** become narrow with a significant reduction in their fluorescence lifetimes. This result can be explained in terms of the fact that structural flexibilities in larger porphyrin rings lead to a large variation in conformations with considerable nonradiative decay channels.

We have evaluated the energy migration efficiencies of the cyclic porphyrin arrays **C10ZA**, **C12ZA**, and **C16ZA** by coincidence measurements. The mean N_C/N_L values of **C10ZA** and **C16ZA** are 0.34 and 0.38, respectively, which are larger than the value of 0.24 found for **C12ZA**. We attribute the less efficient S_1-S_1 annihilation in **C10ZA** to considerable structural strain due to the smaller ring size. On the other hand, in the case of **C16ZA**, the presence of less favorable structural conformations as well as the longer average interchromophoric distance between diporphyrin subunits may disturb S_1-S_1 annihilation. The small N_C/N_L value for **C12ZA** reveals that the overall structure of **C12ZA** is rigid enough without any significant distortion, leading to efficient FRET. The 1,3-phenylene spacer with an angle of 120° between the two linking C−C bonds at 1- and 3-positions of the phenyl group is well-suited to accommodate the six diporphyrin subunits to form the hexagonal structure of **C12ZA**.

Conclusions

Recent progress in the synthesis of covalently and noncovalently linked discrete cyclic porphyrin arrays as models of the photosynthetic light-harvesting antenna has been reviewed. Such covalently linked arrays still remain important and useful with respect to chemical robustness, fine-tuning of structures including distance, orientation, and

bridge, and easy manipulation. The efficient EET was observed in these cyclic arrays, but the ultrafast EET processes with rates > $(1\ ps)^{-1}$ that rival those in the natural LH2 were observed only for **CZ4**−**CZ8**. Collectively, these studies help understand the structural requirements for such very fast EET.

In the perspective of metal-mediated assembly, the zinc porphyrins appending pyridine moieties are attractive building blocks, because of relatively large association and a favorable tendency not to spoil the fluorescence of porphyrins. The porphyrin boxes have been shown to serve as a platform to enable very efficient EET processes along the ring circuit. We have also demonstrated that the *meso*-cinchomeronimide appended Zn(II) porphyrin **CID** exhibits high-fidelity self-sorting assembling to form discrete cyclic trimer, tetramer, and pentamer with large association constants through perfect discrimination of enantiomeric and conformational differences of the *meso*-cinchomeronimide substituents. Exclusive formation of the discrete cyclic aggregates without an appreciable amount of polymeric aggregate is also notable, which is probably driven by favorable entropic factors for the formation of cyclic aggregates. Future studies will focus on incorporation of these functional units into more elaborate model systems and exploration of larger cyclic porphyrin arrays.

The work at Kyoto was partially supported by Grants-in-Aid for Scientific Research (No. 19205006, and 20108001 "pi-Space") from the Ministry of Education, Culture, Sports, Science and Technology, Japan. N.A. thanks a Grant-in-Aid for Young Scientists (B) and GCOE program "Integrated Materials Science" for financial support. The work at Yonsei was supported by the Star Faculty and WCU programs (No. 2008-8-1955) from the Ministry of Education, Science and Technology of Korea.

BIOGRAPHICAL INFORMATION

Naoki Aratani was born in 1975 in Nagoya, Japan. He received his BSc (1999), MSc (2001), and Ph.D. (2005) degrees from Kyoto University. He was selected as a Research Fellow of the JSPS in 2001. In 2003, he started an academic career at the Department of Chemistry of Kyoto University as an assistant professor with Prof. A. Osuka, focusing on the design and synthesis of extremely long porphyrin arrays for the exploration of the nature of giant molecules. In 2006, he joined Prof. Omar M. Yaghi's group as a visiting scientist at the UCLA, studying porous crystalline materials. He received the PCCP Award for Young Chemists in 2008.

Atsuhiro Osuka was born in 1954 in Aichi, Japan. He received a BS in chemistry in 1977 and a Ph.D. in 1982 from Kyoto University. In 1979, he started an academic career at Ehime University as an assistant professor. In 1984, he moved to the Department of Chemistry of Kyoto University, where he became a professor of chemistry in 1996. He was also the leader of the CREST project supported by the JST from 2001 to 2007. He received the Japanese Photochemistry Association Award in 1999. His research interests cover many aspects of synthetic approaches toward the artificial photosynthesis and development of porphyrin-related compounds with novel structures and functions.

Dongho Kim (b. 1957) grew up in Seoul, Korea. He received a B.S. in chemistry from Seoul National University (1980) and a Ph.D. from Washington University (1984). After postdoctoral research at Princeton University, he joined the Korea Research Institute of Standards and Science (1986). He moved to Yonsei University (2000), where he is Underwood Professor of Chemistry. Since 2008, he has been leading the Center for Smart Nano-Conjugates through the World Class University Program supported by the Ministry of Education, Science and Technology of Korea.

FOOTNOTES

*To whom correspondence should be addressed. (A.O.) E-mail: osuka@kuchem.kyoto-u.ac.jp. Fax: +81-75-753-3970. (D.K.) E-mail: dongho@yonsei.ac.kr. Fax: +82-2-2123-2434.

REFERENCES

1 McDermott, G.; Prince, S. M.; Freer, A. A.; Hawthornthwaite-Lowless, A. M.; Papiz, M. Z.; Cogdell, R. J.; Isaacs, N. W. Crystal Structure of an Integral Membrane Light-Harvesting Complex from Photosynthetic Bacteria. *Nature* **1995**, *374*, 517–521.

2 (a) Osuka, A.; Maruyama, K. Synthesis of Naphthalene-bridged Porphyrin Dimers and their Orientation-Dependent Exciton Coupling. *J. Am. Chem. Soc*. **1988**, *110*, 4454–4456. (b) Osuka, A.; Maruyama, K.; Mataga, N.; Asahi, T.; Yamazaki, I.; Tamai, N. Geometry Dependence of Intramolecular Photoinduced Electron Transfer in Synthetic Zinc-ferric Hybrid Diporphyrins. *J. Am. Chem. Soc*. **1990**, *112*, 4958–4959.

3 Osuka, A.; Shimidzu, H. *meso, meso*-Linked Porphyrin Arrays. *Angew. Chem., Int. Ed. Engl*. **1997**, *36*, 135–137.

4 Aratani, N.; Osuka, A.; Kim, Y. H.; Jeong, D. H.; Kim, D. Extremely Long, Discrete *meso-meso*-Coupled Porphyrin Arrays. *Angew. Chem., Int. Ed*. **2000**, *39*, 1458–1462.

5 Nakano, A.; Osuka, A.; Yamazaki, I.; Yamazaki, T.; Nishimura, Y. Windmill-like Porphyrin Arrays as Potent Light-Harvesting Antenna Complexes. *Angew. Chem., Int. Ed*. **1998**, *37*, 3023–3027.

6 Nakano, A.; Yamazaki, T.; Nishimura, Y.; Yamazaki, I.; Osuka, A. Three-Dimensionally Arranged Windmill and Grid Porphyrin Arrays by Ag^{I}-Promoted *meso-meso* Block Oligomerization. *Chem.—Eur. J*. **2000**, *6*, 3254–3271.

7 Hori, T.; Nakamura, Y.; Aratani, N.; Osuka, A. Exploration of Electronically Interactive Cyclic Porphyrin Arrays. *J. Organomet. Chem*. **2007**, *692*, 148–155.

8 Maeda, C.; Kamada, T.; Aratani, N.; Osuka, A. Chiral Self-Discriminative Self-Assembling of *meso-meso*-Linked Diporphyrins. *Coord. Chem. Rev*. **2007**, *251*, 2743–2752.

9 Nakamura, Y.; Aratani, N.; Osuka, A. Cyclic Porphyrin Arrays as Artificial Photosynthetic Antenna: Synthesis and Excitation Energy Transfer. *Chem. Soc. Rev*. **2007**, *36*, 831–845.

10 Anderson, S.; Anderson, H. L.; Sanders, J. K. M. Expanding Roles for Templates in Synthesis. *Acc. Chem. Res*. **1993**, *26*, 469–475.

11 Aratani, N.; Takagi, A.; Yanagawa, Y.; Matsumoto, T.; Kawai, T.; Yoon, Z. S.; Kim, D.; Osuka, A. Giant *meso-meso*-Linked Porphyrin Arrays of Micrometer Molecular Length and Their Fabrication. *Chem.—Eur. J*. **2005**, *11*, 3389–3404.

12 Aratani, N.; Osuka, A. Synthesis of *meso-meso* Linked Hybrid Porphyrin Arrays by Pd-Catalyzed Cross-Coupling Reaction. *Org. Lett*. **2001**, *3*, 4213–4216.

13 Shinokubo, H.; Osuka, A. Marriage of Porphyrin Chemistry with Metal-Catalysed Reactions. *Chem. Commun*. **2009**, 1011–1021.

14 Aratani, N.; Osuka, A. A *meso-meso* Directly Linked Octameric Porphyrin Square. *Chem. Commun*. **2008**, 4067–4069.

15 Nakamura, Y.; Jang, S. Y.; Tanaka, T.; Aratani, N.; Lim, J. M.; Kim, K. S.; Kim, D.; Osuka, A. Two-Dimensionally Extended Porphyrin Tapes: Synthesis and Shape-Dependent Two-Photon Absorption Properties. *Chem.—Eur. J*. **2008**, *14*, 8279–8289.

16 Tsuda, A.; Osuka, A. Fully Conjugated Porphyrin Tapes with Electronic Absorption Bands That Reach into Infrared. *Science* **2001**, *293*, 79–82.

17 Kasha, M.; Rawls, H. R.; El-Bayoumi, M. A. The Exciton Model in Molecular Spectroscopy. *Pure Appl. Chem*. **1965**, *11*, 371–392.

18 Nakamura, Y.; Hwang, I.-W.; Aratani, N.; Ahn, T. K.; Ko, D. M.; Takagi, A.; Kawai, T.; Matsumoto, T.; Kim, D.; Osuka, A. Directly *meso-meso*-Linked Porphyrin Rings: Synthesis, Characterization, and Efficient Excitation Energy Hopping. *J. Am. Chem. Soc*. **2005**, *127*, 236–246.

19 Peng, X.; Aratani, N.; Takagi, A.; Matsumoto, T.; Kawai, T.; Hwang, I.-W.; Ahn, T. K.; Kim, D.; Osuka, A. A Dodecameric Porphyrin Wheel. *J. Am. Chem. Soc*. **2004**, *126*, 4468–4469.

20 Hwang, I.-W.; Ko, D. M.; Ahn, T. K.; Yoon, Z. S.; Kim, D.; Peng, X.; Aratani, N.; Osuka, A. Excitation Energy Migration in a Dodecameric Porphyrin Wheel. *J. Phys. Chem. B* **2005**, *109*, 8643–8651.

21 Hori, T.; Aratani, N.; Takagi, A.; Matsumoto, T.; Kawai, T.; Yoon, M.-C.; Yoon, Z. S.; Cho, S.; Kim, D.; Osuka, A. Giant Porphyrin Wheels with Large Electronic Coupling as Models of Light-Harvesting Photosynthetic Antenna. *Chem.—Eur. J*. **2006**, *12*, 1319–1327.

22 Roszak, A. W.; Howard, T. D.; Southall, J.; Gardiner, A. T.; Law, C. J.; Isaacs, N. W.; Cogdell, R. J. Crystal Structure of the RC-LH1 Core Complex from *Rhodopseudomonas palustris*. *Science* **2003**, *302*, 1969–1972.

23 Hori, T.; Peng, X.; Aratani, N.; Takagi, A.; Matsumoto, T.; Kawai, T.; Yoon, Z. S.; Yoon, M.-C.; Yang, J.; Kim, D.; Osuka, A. Synthesis of Nanometer-Scale Porphyrin Wheels of Variable Size. *Chem.—Eur. J*. **2008**, *14*, 582–595.

24 Chi, X.; Guerin, A. J.; Haycock, R. A.; Hunter, C. A.; Sarson, L. D. The Thermodynamics of Self-Assembly. *J. Chem. Soc., Chem. Commun*. **1995**, 2563–2565.

25 (a) Takahashi, R.; Kobuke, Y. Hexameric Macroring of Gable-Porphyrins as a Light-Harvesting Antenna Mimic. *J. Am. Chem. Soc*. **2003**, *125*, 2372–2373.

26 Wu, A.; Isaacs, L. Self-Sorting: The Exception or the Rule. *J. Am. Chem. Soc*. **2003**, *125*, 4831–4835.

27 Tsuda, A.; Nakamura, T.; Sakamoto, S.; Yamaguchi, K.; Osuka, A. A Self-Assembled Porphyrin Box from *meso-meso*-Linked Bis{5-*p*-pyridyl-15-(3,5-di-octyloxy-phenyl)porphyrinato zinc(II)}. *Angew. Chem., Int. Ed*. **2002**, *41*, 2817–2821.

28 Hwang, I.-W.; Kamada, T.; Ahn, T. K.; Ko, D. M.; Nakamura, T.; Tsuda, A.; Osuka, A.; Kim, D. Porphyrin Boxes Constructed by Homochiral Self-Sorting Assembly: Optical Separation, Exciton Coupling, and Efficient Excitation Energy Migration. *J. Am. Chem. Soc*. **2004**, *126*, 16187–16198.

29 Kamada, T.; Aratani, N.; Ikeda, T.; Shibata, N.; Higuchi, Y.; Wakamiya, A.; Yamaguchi, S.; Kim, K. S.; Yoon, Z. S.; Kim, D.; Osuka, A. High Fidelity Self-Sorting Assembling of *meso*-Cinchomeronimide Appended *meso-meso*-Linked Zn(II) Diporphyrins. *J. Am. Chem. Soc*. **2006**, *128*, 7670–7678.

30 Rigler, R.; Orrit, M.; Basché, T. *Single Molecule Spectroscopy*; Springer: Heidelberg, Germany, 2002.

31 Park, M.; Yoon, M.-C.; Yoon, Z. S.; Hori, T.; Peng, X.; Aratani, N.; Hotta, J.-i.; Uji-i, H.; Sliwa, M.; Hofkens, J.; Osuka, A.; Kim, D. Single-Molecule Spectroscopic Investigation of Energy Migration Processes in Cyclic Porphyrin Arrays. *J. Am. Chem. Soc*. **2007**, *129*, 3539–3544.

32 Yang, J.; Park, M.; Yoon, Z. S.; Hori, T.; Peng, X.; Aratani, N.; Dedecker, P.; Hotta, J.-i.; Uji-i, H.; Sliwa, M.; Hofkens, J.; Osuka, A.; Kim, D. Excitation Energy Migration Processes in Cyclic Porphyrin Arrays Probed by Single Molecule Spectroscopy. *J. Am. Chem. Soc*. **2008**, *130*, 1879–1884.